Acta metall. Vol. 36, No. 4, pp. 847–864, 1988
Printed in Great Britain.

0001-6160/88 $3.00 + 0.00

DEFORMATION BEHAVIOUR OF γ'' STRENGTHENED INCONEL 718

M. SUNDARARAMAN, P. MUKHOPADHYAY and S. BANERJEE
Physical Metallurgy Division, Bhabha Atomic Research Centre, Bombay-400 085, India

(*Received* 11 *May* 1987; *in revised form* 10 *August* 1987)

Abstract—This study on deformation mechanisms of a γ'' (DO_{22} structure) strengthened nickel base alloy (Inconel 718) has shown a new type of precipitate shearing mechanism. When the size of γ'' particles exceeds a critical value (~ 10 nm), these precipitates are sheared by the passage of true crystallographic deformation twins which do not destroy the ordered atomic arrangements within precipitate crystals. For smaller precipitates, shearing occurs by the movement of a group of dislocations which enables restoration of order. Consequent to the change in the precipitate shearing mechanism the work hardening rate drops to a lower value (work hardening exponent changing from ~ 0.8 to ~ 0.5) as the deformation twinning mode becomes operative for precipitates with radii larger than about 10 nm. Strengthening due to precipitation has been estimated as a function of the precipitate size, corresponding to different precipitate shearing and precipitate bypassing mechanisms and these results have been compared with the experimental data.

Résumé—Cette étude des mécanismes de déformation d'un alliage à base nickel durci par γ'' (de structure DO_{22}), l'Inconel 718, a mis en évidence un nouveau type de mécanisme de cisaillement des précipités. Quand la taille des particules de γ'' dépasse une valeur critique (~ 10 nm), ces précipités sont cisaillés par le passage de macles de déformation cristallographiques vraies qui ne détruisent pas les arrangements atomiques ordonnés à l'intérieur des cristaux de précipités. Pour des précipités plus petits, le cisaillement a lieu grâce au mouvement d'un groupe de dislocations qui permet la restauration de l'ordre. Suite à cette modification du mécanisme de cisaillement des précipités, la vitesse de consolidation diminue brutalement (l'exposant de la consolidation passe de $\sim 0{,}8$ à $\sim 0{,}5$) quand le mode de déformation par maclage intervient pour les précipités de rayons supérieurs à 10 nm environ. Nous avons estimé le durcissement dû à la précipitation en fonction de la taille des précipités, pour différents mécanismes de cisaillement et de franchissement des précipités. Nous avons comparé ces résultats avec les résultats expérimentaux.

Zusammenfassung—Die Untersuchung der Verformungsmechanismen einer γ''-ausscheidungsgehärteten Legierung auf Nickelbasis (Inconel 718) hat auf einen neuartigen Mechanismus der Scherung von Ausscheidungen hingewiesen. Oberhalb einer kritischen Größe (~ 10 nm) werden diese γ''-Teilchen dadurch geschert, daß echte kristallografische Verformungszwillinge hindurchlaufen, welche die Atomordnung der Ausscheidungen nicht zerstören. Kleinere Ausscheidungen werden durch das Durchqueren von Versetzungsgruppen, die die Ordnung wiederherstellen können, geschert. Als Folge des Wechsels im Schermechanismus fällt der Verfestigungskoeffizient auf einen niedrigeren Wert (Verfestigungsexponent von $\sim 0{,}8$ auf $\sim 0{,}5$), wenn die Teilchengröße ~ 10 nm überschreitet. Die Ausscheidungshärtung wurde als Funktion der Ausscheidungsgröße entsprechend den verschiedenen Mechanismen der Ausscheidungsscherung und des Vorbeigleitens von Versetzungen ermittelt; die Ergebnisse werden mit den experimentellen Daten verglichen.

1. INTRODUCTION

The mechanisms of precipitation hardening in nickel base superalloys have been studied extensively [1–12]. A great majority of precipitation hardenable nickel base superalloys derive their enhanced strength from the precipitation of the γ' phase which has an ordered, simple cubic ($L1_2$) structure. However, there are quite a few nickel–iron base superalloys which are strengthened by the precipitation of the γ'' phase which has an ordered, body centred tetragonal (DO_{22}) structure [11, 12]. A well known example of this class of alloys is the widely used commercial alloy Inconel 718. In this alloy both γ' and γ'' precipitates form and the predominant contribution to precipitation hardening is provided by the latter [12]. The mode of γ'' precipitation in alloys such as this has been examined in detail [13–15]. The deformation mechanisms as well as the deformation microstructures pertaining to γ'' strengthened alloys have also been studied [11, 12, 15–19]. It appears that there exists some difference in opinion regarding the mode of deformation of γ'' hardened alloys. Some workers [15–17] are of the view that deformation occurs in bands rather than by coplanar flow of dislocations and that faults are produced in γ'' particles along the slip planes. In addition to faulting within γ'' precipitates, some evidence indicating the occurrence of

deformation twinning within these particles has also been obtained [17–19]. Oblak *et al.* [11], on the other hand, have suggested that deformation occurs mainly by the motion of doublets and quadruplets of unit dislocations (of the disordered austenite lattice).

The deformation behaviour of Ni_3V, a single phase alloy possessing the DO_{22} structure, has been investigated in some detail by Vanderschaeve and Escaig [20–22]. In the context of these studies, they have considered how the passage of different types of partial dislocations can lead to the formation of different stacking fault configurations in this structure. It is quite instructive to use some of these ideas while analysing the possible dislocation–precipitate interactions in an alloy consisting of a uniform dispersion of DO_{22} precipitates in a disordered face centred cubic matrix. As discussed in the present paper, such an analysis brings out the interesting possibility that the DO_{22} particles may be sheared by the propagation of deformation twins across them. The occurrence of such a process would not disturb the ordered atomic arrangement in the precipitates. That deformation twinning occurs in γ'' bearing alloys such as Inconel 718 has indeed been confirmed in some earlier investigations [17–19]. Against this background, the work described in the present paper was undertaken with a view to examining the microstructure of deformed, γ'' bearing samples of Inconel 718 and to establishing the conditions under which shear propagation across γ'' particles by deformation twinning is possible in this alloy.

The various mechanisms by which a precipitate can interact with a moving dislocation and impede its motion include those resulting in the creation of extra surfaces and those related to elastic interactions. With the former are associated chemical strengthening (creation of additional matrix–precipitate interface), stacking fault strengthening (formation of stacking faults in the precipitate) and order strengthening (formation of antiphase domain boundaries in the precipitate due to the passage of the dislocation through it). Elastic interactions, on the other hand, can cause modulus hardening and coherency hardening. A recent review summarises the voluminous literature pertaining to the mechanisms of precipitation hardening, including the aforementioned [23]. It is interesting to note in this context that the possibility of shearing of ordered precipitates by the occurrence of deformation twinning in these does not seem to have attracted much attention so far. The present paper discusses this mode of dislocation–precipitate interaction in some detail, with reference to the room temperature deformation behaviour of precipitation hardened Inconel 718 alloy.

2. SOME GEOMETRICAL ASPECTS OF DEFORMATION OF DO_{22} CRYSTALS

As illustrated in Fig. 1(a) the body centred tetragonal unit cell of the DO_{22} structure [24] can be regarded as a stacking of two unit cells of the $L1_2$ structure along any one of the cube axes, with an antiphase boundary (APB) between them [20]. The corresponding disordered structure is the A1 (f.c.c.) structure and in the present paper all structural descriptions will be presented in terms of crystallographic indices of this structure, unless otherwise stated. The atomic arrangement on the close packed (111) plane of a DO_{22} crystal [(112) plane in terms of DO_{22} Miller indices], whose tetragonal axis is parallel to the [001] direction, is shown schematically in Fig. 1(b) [24]. Each of these (111) layers maintains the M_3N stoichiometry, where M and N respectively represent the major and the minor species of atoms present in the crystal. The stacking, one over the other, at regular spacings, of six of these layers in such a manner that each layer is displaced with

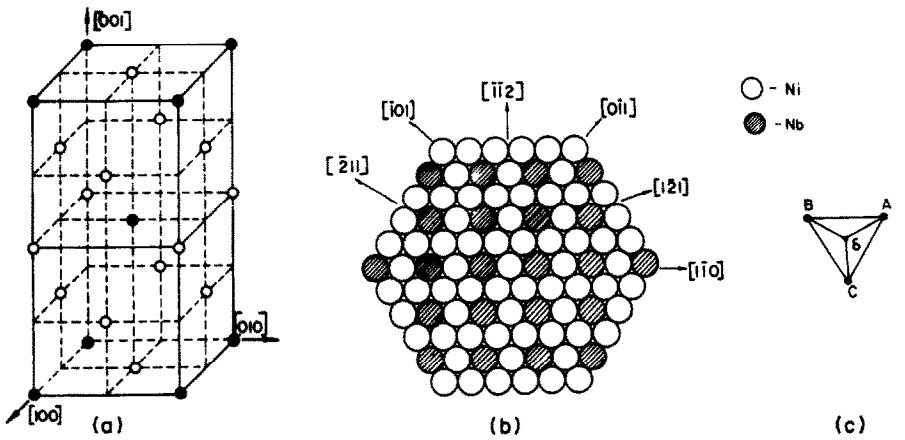

Fig. 1. (a) Unit cell of the DO_{22} structure (γ'' phase-Ni_3Nb); open and filled circles represent nickel and niobium atoms respectively. (b) Atomic arrangement on close packed (111) plane of DO_{22} structure. (c) Part of Thompson tetrahedron for (111) plane.

respect to the preceding one by a $\frac{1}{3}[1\bar{2}1]$ (or a $\frac{1}{3}[\bar{2}11]$) vector, produces the layer stacking sequence characteristic of the DO_{22} structure. This sequence can be represented as $A_1\ B_1\ C_1\ A_2\ B_2\ C_2\ A_1\ B_1 \ldots$ where A_1 and A_2 layers (and similarly, B_1 and B_2 as well as C_1 and C_2 layers) contain atom positions vertically (i.e. along the [111] direction) above one another but the N atom positions do not correspond. A six layer stacking is, therefore, necessary to build this ordered structure.

An inspection of the atomic arrangement on the (111) plane shows that the important lattice translation vectors which can be considered as candidates for dislocation Burgers vectors are

$2\,\mathbf{AB}$ or 2. $\frac{1}{2}[\bar{1}10]$

$3\,\mathbf{C}\delta$ or 3. $\frac{1}{6}[\bar{1}\bar{1}2]$

$4\,\mathbf{BC}$, $4\,\mathbf{AC}$ or 4. $\frac{1}{2}[10\bar{1}]$, 4. $\frac{1}{2}[01\bar{1}]$

$12\,\mathbf{B}\delta$, $12\,\mathbf{A}\delta$ or 12. $\frac{1}{6}[2\bar{1}\bar{1}]$, 12. $\frac{1}{6}[\bar{1}2\bar{1}]$.

The Thompson tetrahedron construction [25] [Fig. 1(c)] has been used in order to specify these vectors. The sequential passage of an appropriate number of similar dislocations, characterised by a resultant Burgers vector equal to any one of the aforementioned vectors, will not introduce any APB or stacking fault in the DO_{22} structure. It should be noted in this context that the three fold rotational symmetry exhibited by the A1 structure is absent in the DO_{22} structure as a consequence of ordering and for this reason, directions such as $\mathbf{A}\delta$, $\mathbf{B}\delta$ and $\mathbf{C}\delta$ or **AB**, **BC** and **CA** are not equivalent.

In view of the large magnitudes of the Burgers vectors associated with the $12\,\mathbf{B}\delta$ or $12\,\mathbf{A}\delta$ dislocations and the correspondingly high self energy values, it is unlikely that these dislocations play any significant role in the deformation process of a phase with the DO_{22} structure. Deformation of such a phase by the movement of a group of similar dislocations with a resultant Burgers vector equal to 4 **BC** or 4**AC** can also be expected to be difficult because of the requirement of a large APB area between the leading and the trailing dislocations. In fact Kirman *et al.* [15] and Chaturvedi *et al.* [12] have not reported any evidence of the operation of this deformation mode. However, Oblak *et al.* [11] have observed the presence of groups of 4 **BC**/**AC** type dislocations in a deformed sample of Inconel 718.

It can be seen from Fig. 1(b) that the passage of a single $\mathbf{C}\delta$ partial dislocation on the (111) plane does not cause any change of the first nearest neighbour atoms but results in the formation of a stacking fault. On the other hand an $\mathbf{A}\delta$ or a $\mathbf{B}\delta$ partial dislocation, during its passage on the (111) plane, produces a complex stacking fault and changes the first nearest neighbour environment. Creation of stacking faults by $\mathbf{C}\delta$ dislocations is, therefore, more likely than by $\mathbf{A}\delta$ or $\mathbf{B}\delta$ dislocations. In the context of the γ'' phase, it is interesting to note that $\mathbf{C}\delta$ dislocations can also play an important role in generating (111) deformation twins as well as the equilibrium δ phase. The former can be produced by the passage of $\mathbf{C}\delta$ dislocations on every (111) plane while the latter can form when these partial dislocations move on every alternate (111) plane. This point will be discussed in greater detail in Section 5.

Let the interaction of matrix dislocations with DO_{22} precipitates distributed in an A1 matrix (a situation similar to that obtained in aged Inconel 718) be now considered, assuming that the DO_{22} tetragonal axis is parallel to the [001] direction in A1. The following dislocation reactions may occur, leading to the formation of partial dislocations:

$$\mathbf{AB} \rightarrow \mathbf{A}\delta + \delta\mathbf{B}$$

$$\mathbf{BC} \rightarrow \mathbf{B}\delta + \delta\mathbf{C}$$

$$\mathbf{CA} \rightarrow \mathbf{C}\delta + \delta\mathbf{A}.$$

Neither of the two partials produced by the first reaction can glide on the (111) plane of a DO_{22} particle without creating complex faults. But the second and the third reactions respectively generate $\delta\mathbf{C}$ and $\mathbf{C}\delta$ partials whose passage through a DO_{22} precipitate results in the formation of a stacking fault. This mode of deformation has been considered by Kirman and Warrington [15]. As far as **AB** dislocations are concerned, it appears that the easiest mode of their propagation through DO_{22} precipitates is by the movement of a dislocation pair and experimental evidences of such coupled motion of two **AB** dislocations have indeed been recorded [11, 12].

It must be emphasised in this context that a given matrix dislocation will interact differently with the different variants of DO_{22} crystals. For instance, the motion of a pair of $\frac{1}{2}[\bar{1}10]$ dislocations on the (111) plane conserves order only in that precipitate variant whose tetragonal axis is parallel to [001]. For order to be conserved in the other two variants (with tetragonal axes parallel to [100] and [010] respectively) coupled motion of groups of four such dislocations has to occur.

3. EXPERIMENTAL

Inconel 718 was obtained in sheet form (of 7 mm thickness) from International Nickel Company. The chemical composition of the alloy is shown in Table 1. The as received material was cold rolled to a thickness of 0.75 mm and pieces of suitable dimensions were obtained from this strip for electron microscopy studies and for tensile testing. All samples, encapsulated in silica tubes under a helium atmosphere, were solutionised at 1373 K for a period of 1 h and then water quenched. Ageing of the solutionised samples was carried out at different periods of time to precipitate γ'' particles of different sizes (see Table 2). The average γ'' particle size corresponding to any given ageing treatment was

Table 1. Chemical composition of Inconel 718

Element	Concentration (wt%)
Ni	52.67
Cr	18.37
Fe	18.18
Nb	6.00
Mo	2.93
Al	0.50
Ti	0.95
Mn	0.20
Si	0.20
C	0.04

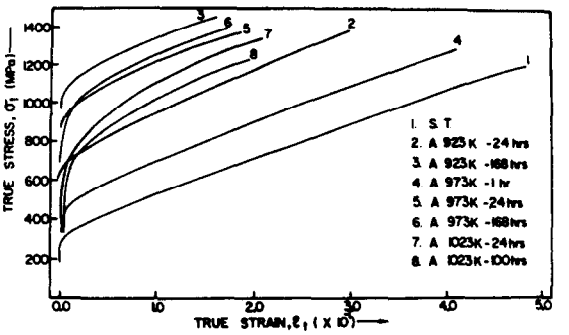

Fig. 2. True stress (σ_t) vs true strain (ϵ_t) plots for Inconel 718 in solution treated (S.T.) and in solution treated and subsequently aged (A) conditions. The temperature and duration of ageing are indicated in the figure.

determined from dark field transmission electron micrographs obtained by using {100} and {1½0} type superlattice reflections with the foil oriented in a ⟨001⟩ orientation. Heat treated samples were deformed at room temperature in air in a floor model Instron machine, using a strain rate of $6.67 \times 10^{-4}\,s^{-1}$. Samples were jet thinned in a Tenupol unit, using an electrolyte containing 1 part perchloric acid and 4 parts ethanol, at a current density of $0.35\,A/cm^2$ at 233 K. The jet thinned samples were examined in a Siemens Elmiskop 102 transmission electron microscope.

4. RESULTS

4.1. Flow behaviour

True stress versus true strain plots for solution treated and aged samples of Inconel 718 are shown in Fig. 2. On the basis of their general appearance, these flow curves could be classified essentially into two groups: those showing a nearly linear behaviour and those exhibiting a parabolic flow behaviour. In order to analyse the room temperature flow behaviour of this alloy, the work hardening parameters were evaluated by following Crussard and Jaoul's formulation [26] in which the true flow stress, σ_t, is expressed as

$$\sigma_t = \sigma_0 + h\epsilon_t^n \qquad (1)$$

where ϵ_t represents the true plastic strain. The values of σ_0 (stress corresponding to $\epsilon_t = 0$), the coefficient, h and the strain hardening exponent, n, obtained from flow curves corresponding to different heat treatment conditions, are listed in Table 2. Also listed in this table are the increments, brought about by precipitation, in the shear stress values, $\Delta\tau$, at 0.2% plastic strain and the average sizes (mean radius) of γ'' precipitates corresponding to different ageing treatments. The value of Taylor's orientation factor was assumed to be 3.06 [27] for converting tensile stress to shear stress. Such an analysis established the fact that the strain hardening coefficients associated with these specimens could be broadly classified into two groups, one with $n \sim 0.85$ and the other with $n \leqslant 0.57$. The former corresponded to the solution treated microstructure and to microstructures with a distribution of very fine particles (smaller than about 10 nm in radius) in the supersaturated matrix while the latter was associated with microstructures containing γ'' precipitates of sizes larger than a critical size of ~ 10 nm.

4.2. Microstructure produced by solution treating and ageing

It was found that the solution treatment used (soaking at 1373 K for 1 h, followed by water quenching) in this work produced an essentially single phase microstructure, with a sparse dispersion of primary carbide particles in the supersaturated austenite. The solution treated alloy contained a fairly high density of dislocations which were presumably generated by quenching stresses. Most of these dislocations were noticed to be arranged in planar arrays on {111} planes (Fig. 3). Application of the $\mathbf{g}\cdot\mathbf{b}$ visibility criterion in conjunction with single surface trace analysis demonstrated that these dislocations, in gen-

Table 2. Work hardening parameters and increment in flow stress as a function of γ'' particle size

Heat treatment	γ'' particle size R (nm)	0.2% Y.S. σ (MPa)	Percent elongation	Increment in flow stress $\Delta\tau$ (MPa)	σ_0 (MPa)	h (MPa)	n
S.T.—1373 K—1 h	Not present	280	63.3	—	298	1696	0.895
S.T.—A 973 K—1 h	Unresolved	419	48.7	45.4	415	1734	0.804
S.T.—A 923 K—24 h	2.0	642	36.0	118.3	650	1956	0.837
S.T.—A 923 K—168 h	10.0	985	15.3	231.0	915	1092	0.427
S.T.—A 973 K—24 h	12.0	938	18.6	214.8	896	1432	0.532
S.T.—A 973 K—168 h	28.0	820	18.2	176.0	581	1273	0.286
S.T.—A 1023 K—24 h	35.0	580	24.6	98.0	610	1749	0.556
S.T.—A 1023 K—100 h	60.0	490	23.4	68.6	604	1562	0.566

S.T.—solution treated; A—aged.

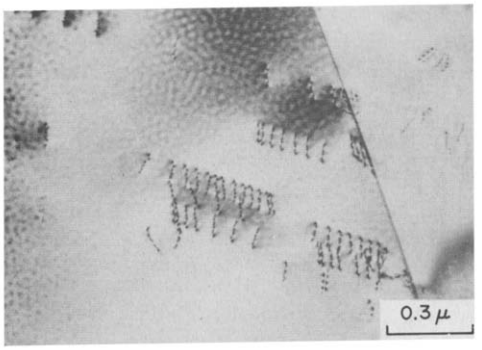

Fig. 3. Microstructure of the solution treated (1373 K for 1 h and water quenched) alloy showing planar arrangement of dislocations along an (111) plane.

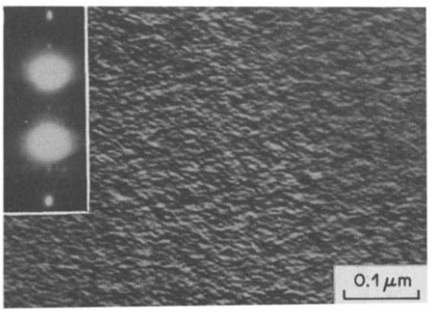

Fig. 4. Microstructure of the aged (973 K for 1 h) alloy showing a mottled contrast under a two beam imaging condition (g = 200). The inset shows the operating reflection and the presence of DO_{22} superlattice reflections.

eral, had Burgers vectros of the type $\frac{1}{2}\langle\bar{1}10\rangle$ and a mixed character.

A mottled contrast could be observed in TEM bright field images obtained from samples aged for 1 h at 973 K following the solution treatment (Fig. 4). No clearly discernible precipitates could be resolved but diffraction patterns showed the presence of weak DO_{22} superlattice reflections. Attempts to resolve precipitates in dark field images obtained by using these reflections were unsuccessful. Distinctly resolvable precipitates were found in samples aged for 24 h at 973 K. These precipitates, which could be identified to be of the γ'' phase, were homogeneously distributed and ellipsoidal in shape (Fig. 5). Streaking

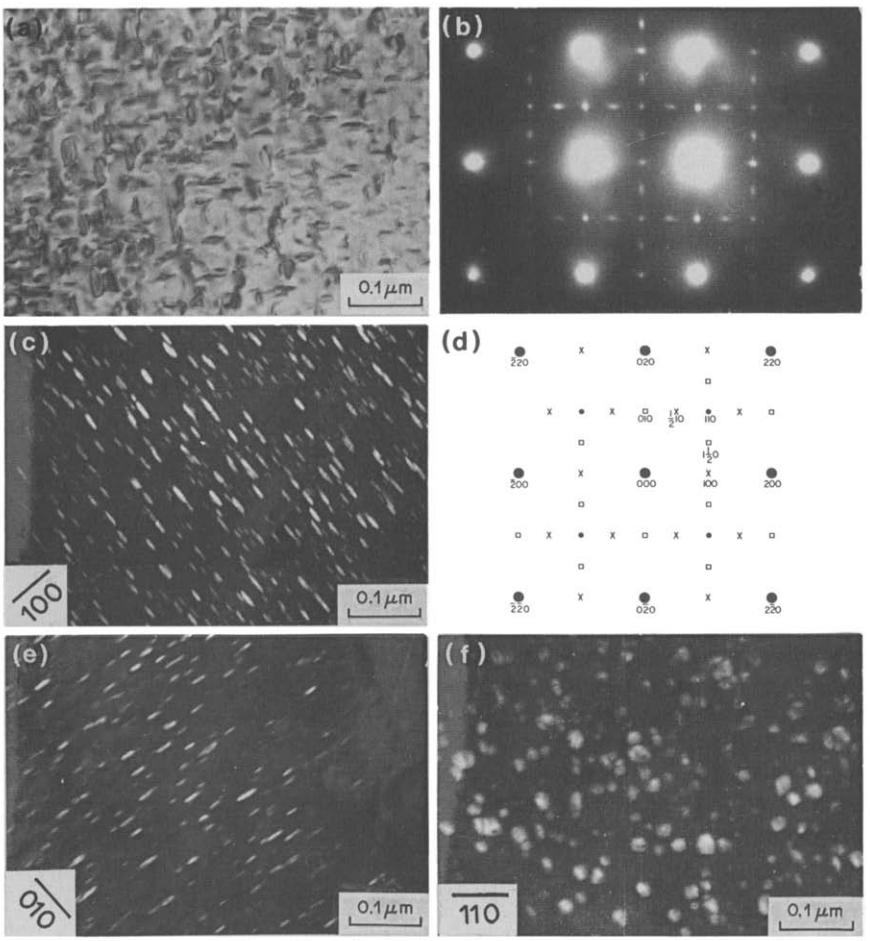

Fig. 5. Bright field micrograph (a) of the alloy aged at 973 K for 24 h shows the distribution of three variants of γ'' precipitates. (b) SAD [001] zone axis. (d) Corresponding key. Different variants are separately imaged in dark field micrographs taken with g = 100 (c), g = 010 (e), and g = 110 (f).

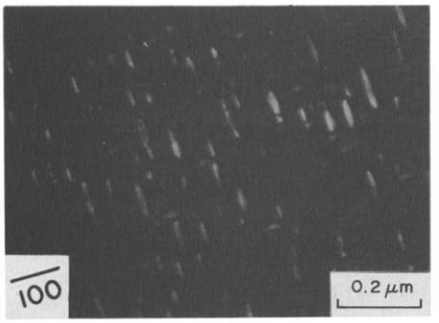

Fig. 6. Dark field micrograph taken with $\mathbf{g} = 100$ shows both ellipsoidal γ'' and spherical γ' precipitates in the alloy aged at 1023 K for 24 h.

was observed in diffraction patterns corresponding to $\langle 001 \rangle$ zone axes [e.g. Fig. 5(b)] and dark field imaging with the steaked $\{100\}$ superlattice reflections brought only those precipitate variants, which lay normal to the direction of streaking, in contrast. This suggested that the habit plane of the γ'' precipitates was perpendicular to the tetragonal axis. On the basis of the available lattice parameter data [11], it is known that a tetragonal distortion of about 2.5% is produced along this direction due to the $A1 \rightarrow DO_{22}$ transformation. The distortions along the other two $\langle 100 \rangle$ directions, which lie on the habit plane, are extremely small ($\sim 0.5\%$).

In addition to the ellipsoidal γ'' particles, some spherical precipitates were also seen in dark field images with $\{100\}$ reflections (Fig. 6). These precipitates have been observed earlier in aged Inconel 718 and the corresponding phase has been identified to be the γ' phase [$Ni_3(Al, Ti)$, $L1_2$ structure] [13, 28]. In electron diffraction patterns, all superlattice reflections associated with the γ' precipitates coincide with one or the other of those appearing due to the three variants of the γ'' precipitates and these two types of particles can be distinguished only by their shapes in appropriate dark field imaging. The strain configurations associated with the precipitation of these two phases in the austenite matrix are responsible for dictating a spherical (often cuboidal after sufficient growth) shape for γ' and an ellipsoidal shape for γ'' particles. In the present work, the ratio of the volume fractions of the γ' and the γ'' phases was found to be about 1:4. It was also noted that even though these precipitates grew to fairly large sizes on prolonged ageing at 1023 K, they continued to remain coherent with the matrix.

4.3. Deformation microstructure of solution treated alloy

In order to study the post deformation dislocation structures produced in the solution treated alloy, samples deformed to 2% plastic strain and to 60% plastic strain were examined. In both cases, predominantly planar dislocation arrangements were observed, though dislocation tangling occurred to some extent in the heavily deformed samples, unlike in the lightly deformed ones (Fig. 7). On the whole, however, the deformation even in the former case appeared to be confined mainly within planar slip bands. It was also noted that in spite of the strong tendency for planar slip, dislocations in the deformed alloy did not show any resolvable splitting into partials.

4.4. Microstructure of aged alloy subjected to small deformations

Samples aged at 1023 K (for periods sufficiently long to bring about precipitation) and subsequently deformed to 2% plastic strain showed a variety of dislocation configurations which included the following.

(i) Circular dislocation loops often appeared around spherical γ' particles [e.g. regions marked A in Fig. 8(a)].
(ii) A large number of dislocation pairs were noticed and these were generally associated with γ'' particles [e.g. regions marked B in Fig. 8(a)].
(iii) Some of the dislocations were observed to split up into partial dislocations on entering γ'' precipitates [e.g. region C in Fig. 8(b)].

Apart from exhibiting these dislocation structures, the aged and lightly deformed specimens also showed

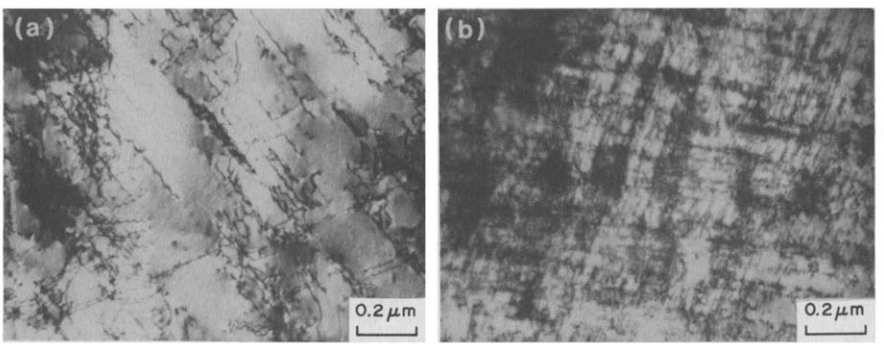

Fig. 7. Accumulation of dislocations primarily along $\{111\}$ slip planes in solution treated alloy subjected to (a) 2% and (b) 60% plastic strain.

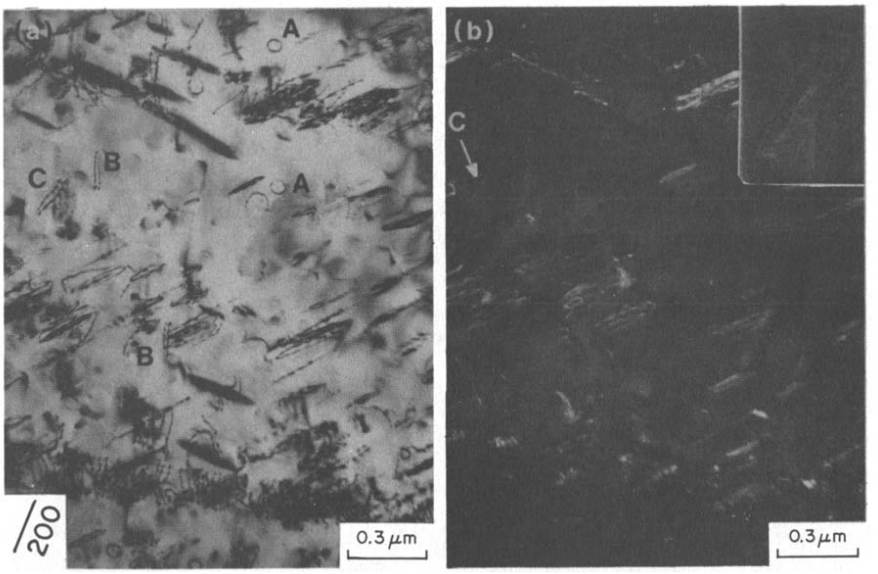

Fig. 8. Microstructure of the alloy aged at 1023 K for 130 h and subsequently deformed to 2% plastic strain showing dislocation–precipitate interactions. (a) Bright field with $\mathbf{g} = 200$. (b) Dark field with $\mathbf{g} = \bar{2}00$. Inset shows magnified view of region marked C. Specific dislocation interactions are discussed in the text.

some deformation induced faulting of γ'' precipitates (indicated by arrows in Fig. 9). The fact that these faults were introduced during the process of deformation and not as a consequence of precipitate growth was confirmed by their occurrence along deformation bands (regions marked A in Fig. 9), and by their relative scarcity in specimens aged but not subsequently deformed. The offset produced on γ'' particles due to the passage of deformation bands indicated that these precipitate regions contained multilayered stacking faults. Two sets of deformation bands, lying on two different {111} slip plane variants, could be observed in Fig. 9 (one set marked A and other set marked by arrows). Another point that warrants mention in the context of the lightly deformed samples is that though dislocation pairs were frequently noticed in these samples, no evidence for the occurrence of dislocation quartets, reported by Oblak *et al.* [11], could be obtained.

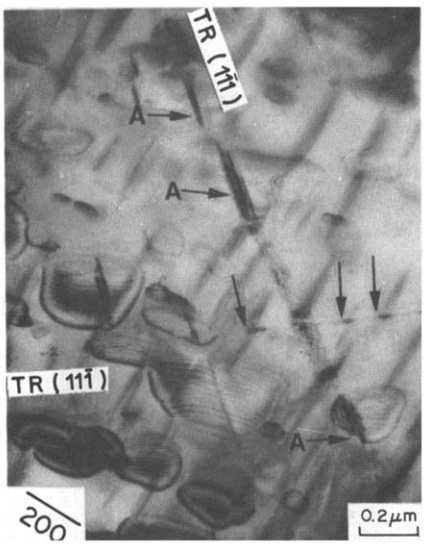

Fig. 9. Stacking faults produced within γ'' precipitates due to deformation (2% plastic strain) of aged (1023 K for 130 h) samples imaged in bright field ($\mathbf{g} = 200$). The association of stacking faults within γ'' with the deformation bands along {111} planes can also be noticed.

Identification of the Burgers vectors of the dislocations bounding the stacking faults within γ'' precipitates was attempted, by imaging the same precipitate in the dark field, using different operating reflections (Fig. 10). The fault plane was determined, by stereographic analysis, to be (111). The expected contrasts under different operating reflections, for the **A**δ, **B**δ and **C**δ partial dislocations, are summarised in Table 3. It was found that one of the partials bounding the fault satisfied the invisibility criterion with $\mathbf{g} = (\bar{1}31)$ [Fig. 10(b)] while the other did not satisfy this criterion with $\mathbf{g} = (\bar{2}02)$ [Fig. 10(c)]. It could be inferred, therefore, that these two partial dislocations were respectively of the **C**δ and the **B**δ types. It could be seen on the basis of the discussion in Section 2, that only the former could glide through the precipitate, leading to the formation of a stacking fault within it, while the latter would remain pinned to the precipitate–matrix interface.

4.5. Microstructure of aged alloy subjected to large deformations

TEM observations made on aged samples subjected to deformations leading to large plastic strains will be reported in this section. The microstructures developed could be grouped into two categories,

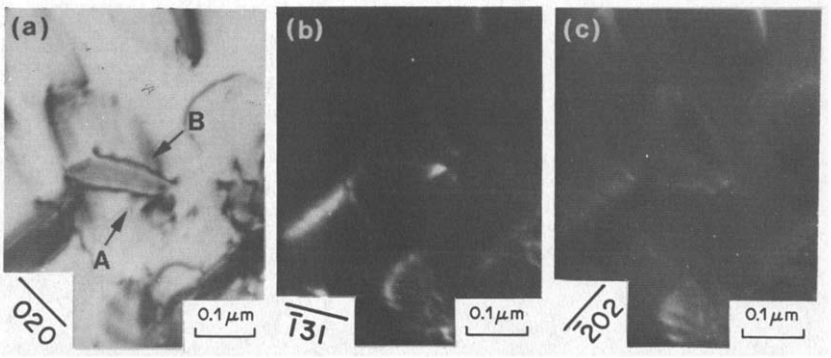

Fig. 10. Contrast analysis of dislocations bounding stacking faults within a γ'' precipitate in the alloy aged at 1073 K for 48 h. The dislocations marked A and B are visible in bright field ($\mathbf{g} = 020$) image (a), and the dark field ($\mathbf{g} = \bar{2}02$) image (c) while only the dislocation A is visible in the dark field image taken with $\mathbf{g} = \bar{1}31$ (b).

depending on whether γ'' particles underwent deformation twinning or not. In fact, the occurrence of deformation twinning within these precipitates was found to be related to their size.

The typical microstructure of a sample, aged at 973 K for 24 h to produce a dispersion of fine γ'' precipitates, and subsequently deformed to about 19% plastic strain is shown in Fig. 11(a). A distribution of deformation bands along the {111} planes could be seen in micrographs such as this. The corresponding SAD patterns [e.g. Fig. 11(b)] testified to the presence of deformation twins within these bands. In these patterns streaks occurred along directions perpendicular to the {111} planes and, within these streaks, intensity maxima were present at locations which corresponded to the {111} twin reflections. Dark field imaging using such a twin reflection [Fig. 11(c)] was found to bring the twin lamellae as well as parts of some γ'' precipitates in bright contrast. Precipitates were not visible within the deformation bands in dark field images obtained by using the {001} superlattice reflections [e.g. Fig. 11(d)].

Deformation structures of samples aged for longer periods (e.g. 168 h at 973 K), and thus containing relatively coarse precipitates (~ 60 nm diameter along the major axis), showed that the γ'' particles had apparently been fragmented into slices along the {111} planes (Fig. 12). SAD patterns obtained from regions containing such precipitates showed streaking

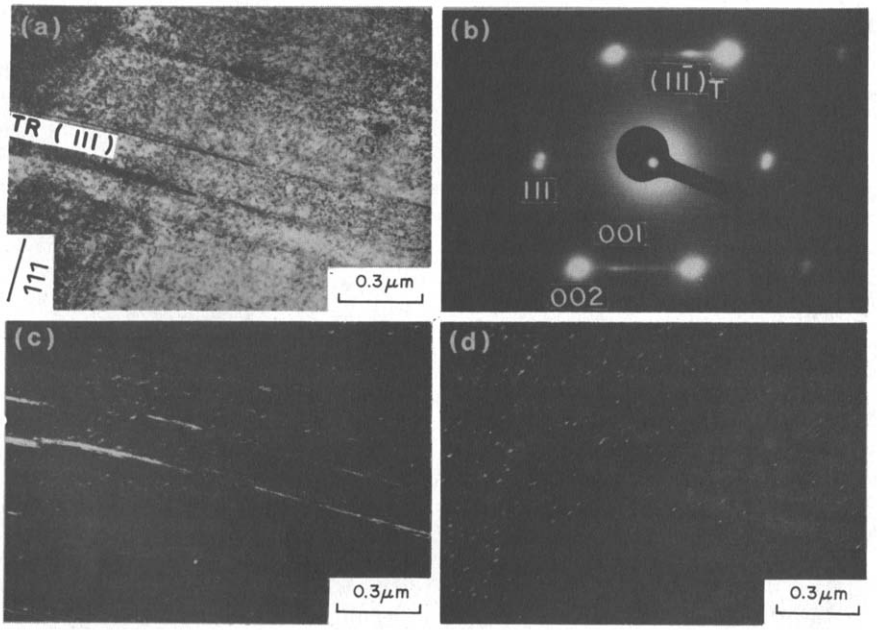

Fig. 11. Microstructures of Inconel 718 sample (aged at 973 for 24 h) deformed to 19% plastic strain. (a) Bright field micrograph; (b) corresponding diffraction pattern ([$1\bar{1}0$] zone axis) showing twin reflections. (c) Dark field imaging with twin reflection [$\mathbf{g} = (11\bar{1})_T$] brings twin segments within deformation bands in bright contrast. (d) Dark field image with superlattice reflection ($\mathbf{g} = 001$) shows the absence of γ'' precipitates within deformation bands.

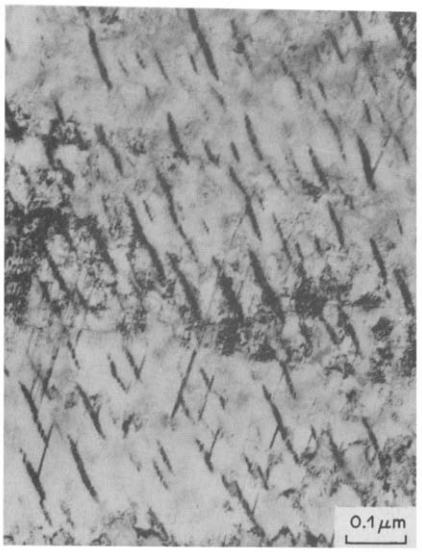

Fig. 12. Deformation (18% plastic strain) of the alloy aged at 973 K for 168 h is seen to have produced microtwins within γ'' precipitates.

along the $\langle 111 \rangle^*$ directions in the reciprocal space. This is illustrated in the diffraction pattern, with $[1\bar{1}0]$ zone axis, presented in Fig. 13(a). The extra spots along these streaks could be identified as twin reflections. It is interesting to note that superlattice reflections corresponding to twinned segments of γ'' particles also appear in this pattern, viz. the appearance of the $(001)_{\gamma''}$ twin reflection midway between the (000) spot and the $(002)_T$ twin spot. This type of association of superlattice twin reflections with matrix twin reflections clearly demonstrated that deformation twinning of γ'' precipitates conserved order within the twin bands and, therefore, corresponded to a true crystallographic twinning. It could also be inferred, from evidences such as this, that the matrix–precipitate lattice correspondence for the twinned regions was the same as that for the twin free regions.

Dark field images obtained by using the $(002)_T$ twin reflection [e.g. Fig. 13(b)] revealed several important features, as described in the following.

(i) Some matrix twin segments (marked X) appeared to propagate through a few γ'' precipitates. The average length of these twin segments was about 0.2 μm and even though these extended through the matrix as well as a few precipitates, no detectable deviation at the points of intersection with the precipitates could be noticed.

(ii) Serrated habit planes of γ'' particles belonging to the [001] variant (marked Y) were suggestive of fragmentation of these precipitates. Individual slices of deformation twins within these precipitates could not be resolved in this foil orientation ($[1\bar{1}0]$ zone axis) since the projected image of each overlapped on those of neighbouring slices.

(iii) The habit plane of the [001] variant of the γ'' precipitates was found to be inclined to the [001] matrix direction by an angle of about 13°. This pointed to the fact that the offsets caused by deformation twinning led to a rotation of the macroscopic (or average) γ'' habit plane by about 13° with respect to the normal habit plane (parallel to the (001) matrix plane).

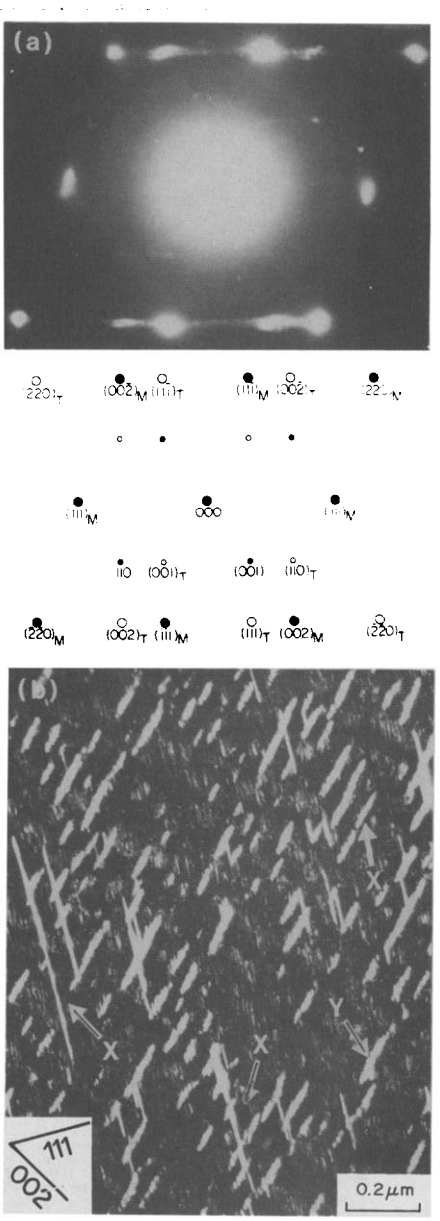

Fig. 13. Deformation microstructure of a sample aged at 973 K for 168 h. (a) $[1\bar{1}0]$ SAD pattern shows superlattice reflection mid way between (000) and $(002)_T$ reflection suggesting that the twinned crystals generated in the deformation process are also ordered. Dark field micrograph taken with $\mathbf{g} = (002)_T$ (b) shows the distribution of microtwins within different variants of γ'' precipitates. A few segments of matrix twin can also be noticed.

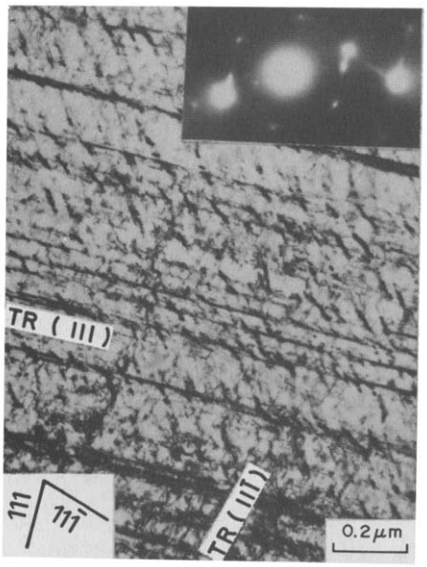

Fig. 14. Bright field micrograph shows deformation bands along two variants of {111} planes in an aged (973 K for 168 h) sample deformed to 18% plastic strain. Inset (SAD pattern) shows evidence for γ'' twinning along these two planes.

(iv) γ'' precipitates belonging to the [100] and the [010] variants (which were indistinguishable in the [1$\bar{1}$0] foil orientation) showed only thin, parallel lamellae in contrast in dark field imaging with the fundamental $(002)_T$ reflection.

It could thus be seen that all the three precipitate variants contained closely spaced lamellae which corresponded to twinned γ'' orientations. Since the precipitate orientations prior to twinning did not give rise to a diffracted spot at the $(002)_T$ location, it could be concluded that all the lamellae which were in bright contrast in dark field images formed by using this reflection [e.g. Fig. 13(b)] corresponded to new orientations which were generated within the precipitates due to deformation twinning.

A high density of deformation bands along conjugate {111} planes and the resulting fragmentation of γ'' particles by deformation twinning (Fig. 14) were also observed in some regions of the aged and heavily deformed samples.

Figure 15 illustrates how the γ'' precipitates are sliced along different {111} planes as a consequence of post-precipitation deformation. The bright field micrograph [Fig. 15(a)] shows internally twinned particles distributed homogeneously within the matrix. It could be seen that precipitates belonging to a specific variant contained twins predominantly along a specific {111} type plane, though intersecting twins on conjugate {111} planes were also noticed within some precipitates [marked by arrows in Fig. 15(a)]. These micrographs demonstrate that each precipitate variant was associated with a favoured twin plane (of the type {111}). The selection of this plane was presumably dictated by the relative orientation of the stress axis.

The fragmentation of γ'' particles due to twinning resulted in slicing of precipitate planes along {111} planes. Since the average thickness of each slice was only about 10 nm, pronounced streaking along ⟨111⟩ reciprocal lattice directions was noticed in addition to the ⟨100⟩ streaking perpendicular to the habit plane of the precipitates. Figure 16 shows one such diffraction pattern where streaking of {110} type spots along the [$\bar{1}$10] direction is consistent with the geometry of the precipitates sliced along ($\bar{1}$11)

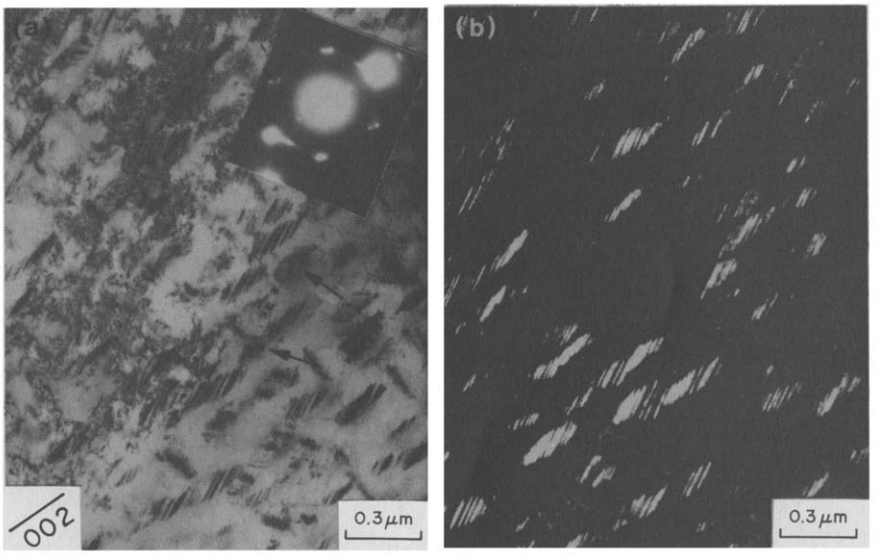

Fig. 15. (a) Bright field micrograph and (b) corresponding dark field micrograph taken with a fundamental twin reflection [$\mathbf{g} = (111)_T$] in a sample aged at 1023 K for 24 h and then deformed show that a specific variant of twinning is predominantly operative within a given variant of γ'' precipitates.

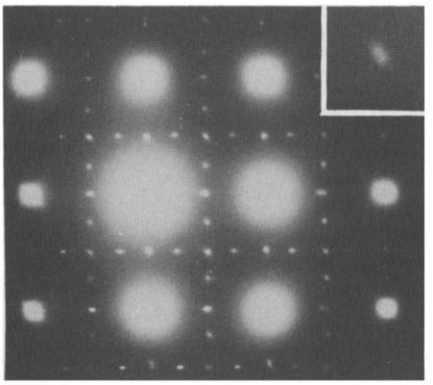

Fig. 16. [001] diffraction pattern from a sample aged at 973 K for 168 h and deformed to 18% plastic strain shows detectable streaking of {110} spots along [1$\bar{1}$0] directions in the reciprocal space [key to SAD is the same as in Fig. 5(d)]. Inset shows magnified view of a {110} spot.

and (1$\bar{1}$1) planes. No extra reflections due to twins would be visible in this orientation unless the foil is buckled [29].

Extensive deformation bands were observed in samples aged at 973 K for 1 h and at 923 K for 24 h and subsequently deformed respectively to 48 and 36% plastic strains. An example is shown in Fig. 17. However, deformation twinning was not found to occur in these samples in which the γ'' particle size was extremely fine. S.A.D. patterns obtained from regions containing deformation bands (see inset) did not contain any twin reflection. This observation was quite different from those made on samples containing larger γ'' particles and implied that deformation twinning occurred only when the precipitate size exceeded a certain critical value. Individual dislocations within the deformation bands could be resolved in many instances [e.g. Fig. 17(b)].

5. DISCUSSION

5.1. Deformation microstructure of solution treated alloy

A noteworthy feature of the microstructure of the solution treated as well as of the solution treated and deformed alloy was that dislocations were invariably arranged in planar arrays. Apparently cross slip of dislocations, leading to tangling and cell formation, was almost absent. Such a situation would arise if the stacking fault energy (SFE) of the alloy was sufficiently low to inhibit cross slip or if short range order (SRO) existed even in the solution treated material or if both these conditions were simultaneously present.

Though unalloyed nickel has a high SFE [30], it is known that alloying additions of elements like chromium, molybdenum, aluminium and titanium can bring down the value of this parameter substantially [31–33]. In view of the composition of Inconel 718, it is, therefore, quite likely that the SFE of this alloy is much lower than that of nickel. It should be noted, however, that the dislocation images indicated that the SFE value was not so low as to lead to the formation of stacking faults bounded by widely separated partial dislocations. From the knowledge of the various elements present in this alloy, the SFE was roughly estimated to be 75 mJ/m^2 (compared with 50 mJ/m^2 reported by Fournier and Pineau [18]). Though these values should be regarded as approximate ones, they point to the fact that this alloy is one of the intermediate SFE nickel base alloys. A common feature of these alloys is that dislocations in these are arranged in planar arrays [31].

The solution treatment temperature used in this work (1373 K) was much higher than the dissolution temperatures of the ordered intermetallic phases that form in Inconel 718 [34]. However, it is possible that some degree of SRO existed in the solution treated and quenched alloy.

5.2. Stacking fault energy of the γ'' phase

Stacking faults were quite frequently observed within γ'' precipitates in deformed as well as undeformed specimens [15]. This suggested that the SFE of the γ'' phase in Inconel 718 is quite low. It has been reported that in the nickel–vanadium system, the equilibrium Ni_3V phase has a fairly low SFE

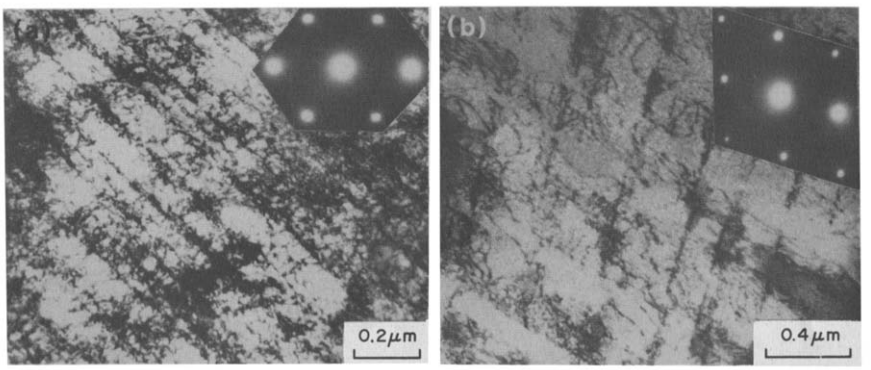

Fig. 17. Deformation microstructures observed in samples containing extremely fine γ'' precipitates show absence of twinning as evidenced from the absence of twin reflections in the diffraction patterns (inset). (a) Corresponds to ageing at 973 K for 1 h and then deformed to 48% plastic deformation and (b) corresponds to ageing at 973 K for 24 h and then deformed to 36% plastic strain.

(22 mJ/m^2) and that the introduction of the associated stacking faults does not produce any order faults [21]. Since the metastable γ'' (Ni_3Nb) phase in Inconel 718 is isostructural with Ni_3V, both the phases having the DO_{22} structure, and since niobium and vanadium belong to the same group (VB) in the periodic table, it may not be unreasonable to assume that the SFE of these two intermetallic phases are quite similar. Experimental determination of SFE in the γ'' phase could not be undertaken in the present work because the coherent γ'' particles could not be grown to sufficiently large sizes to ensure the attainment of the equilibrium separation between the partials bounding a stacking fault.

5.3. *Deformation of γ'' and γ' precipitates*

5.3.1. Superdislocations. The fact that matrix dislocations in samples aged at 1023 K for 130 h often appeared in pairs [Fig. 8(a)] suggested that these dislocations glided through the ordered precipitates. The atomic arrangement on the (111) plane of the DO_{22} structure [Fig. 1(b)] indicates that the shortest lattice translation vectors on this plane are $\frac{1}{2}[\bar{1}\bar{1}2]$ or 3 **C**δ and $[\bar{1}10]$ or 2 **AB**. As discussed in Section 2, when a pair of $\frac{1}{2}[\bar{1}10]$ dislocations pass through γ'' particles belonging to an appropriate orientation variant, no order faults are produced. **AB** dislocations may thus cross these γ'' precipitates and emerge in the matrix as dislocation pairs. The observed paired dislocations presumably corresponded to this situation.

The average γ' particle diameter in samples subjected to this ageing treatment (130 h at 1023 K) was about 40 nm. It was seen that the γ' precipitates in the aged and deformed samples were generally associated with Orowan loops. No evidence of the presence of superdislocations in the vicinity of these particles was obtained. In order to verify theoretically whether looping would be the major mode of deformation for the above mentioned γ' particle size, the increment in flow stress was calculated by using the formulae derived by Hulther *et al.* [9] and by Hirsh *et al.* [35] for particle shearing and looping respectively. It was assumed that the volume fraction of the γ' was 0.05 [12], that the APB energy of γ' in this alloy was 175 mJ/m^2 [11] and that the value of Poisson's ratio, ν, was 1/3. The calculated value of the increase in flow stress for particle looping was only 115 MPa as compared with 152 MPa for particle shearing. On the basis of these estimates, it would be expected that dislocations would bypass γ' particles of diameters larger than about 40 nm by looping around them in conformity with the experimental observations. This suggested that the observed pairs of dislocations were mainly associated with γ'' particles.

5.3.2. Stacking faults. As mentioned in Section 2, the shearing of γ'' precipitates belonging to the [001] variant (i.e. c axis parallel to [001]) can also occur, without the formation of an order fault or a stacking fault, by the passage of a group of dislocations whose resultant Burgers vector equals 3 **C**δ. Such dislocations, which can form by a combination of **CA** and **CB** dislocations gliding on the same or on neighbouring slip planes, may dissociate into two partials separated by an intrinsic stacking fault by the dislocation reaction [21]

$$3\,\mathbf{C}\delta \rightarrow 2\,\mathbf{C}\delta + \mathbf{C}\delta.$$

A dislocation configuration comprising three **C**δ partials can, therefore, cut across γ'' particles without disrupting either the order or the stacking sequence. The presence of such dislocation configurations (triplet of **C**δ partials) has, in fact, been noticed in the equilibrium Ni_3V phase [21]. However, in the present work, the occurrence of such triplets was not observed even though a large number of deformed samples of aged Inconel 718 were carefully scanned.

The frequent occurrence of stacking faults within the γ'' precipitates in the lightly deformed alloy implied that particle shearing by the passage of **C**δ partials was a favoured deformation mode. It should be reiterated, in this context, that such a shear (with a displacement vector $\frac{1}{6}\langle 112\rangle$) produces a stacking fault without changing the first nearest neighbour environment. The frequent incidence of faulting in γ'' particles in a deformed alloy of composition similar to that of Inconel 718 has been reported earlier by Kirman and Warrington [15]. However, Oblak *et al.* [11] did not come across faulted γ'' precipitates in their study on Inconel 718. They argued that the $\frac{1}{6}\langle 112\rangle$ shear is restricted in this alloy because of the presence of γ' precipitates in which creation of complex faults occurs owing to the passage of **C**δ dislocations. But the observations made in the present work clearly demonstrated that stacking faults were indeed formed in the γ'' particles in the aged and lightly deformed alloy, in spite of the presence of a significant volume fraction of γ' precipitates.

5.3.3. Deformation twins. A particularly noteworthy feature of the microstructure of heavily deformed samples containing relatively coarse γ'' precipitates (larger than ~10 nm along the major axis) was the profuse deformation twinning of these particles. The abundance of deformation twins within these precipitates indicated that precipitate shearing could occur quite easily by deformation twinning. An analysis of the crystallography of twinning in the DO_{22} structure is very relevant in the context of this observation.

Table 3. Visibility of Aδ, Bδ and Cδ dislocations under different reflections

Operating reflection	Partials on (111) fault plane A$\delta = \frac{1}{6}[\bar{1}2\bar{1}]$	B$\delta = \frac{1}{6}[2\bar{1}\bar{1}]$	C$\delta = \frac{1}{6}[\bar{1}\bar{1}2]$
020	V	V	V
$\bar{1}31$	V	V	I
$\bar{1}11$	V	V	V
$\bar{2}02$	I	V	V
$\bar{1}\bar{1}1$	V	V	V

V—visible; I—invisible.

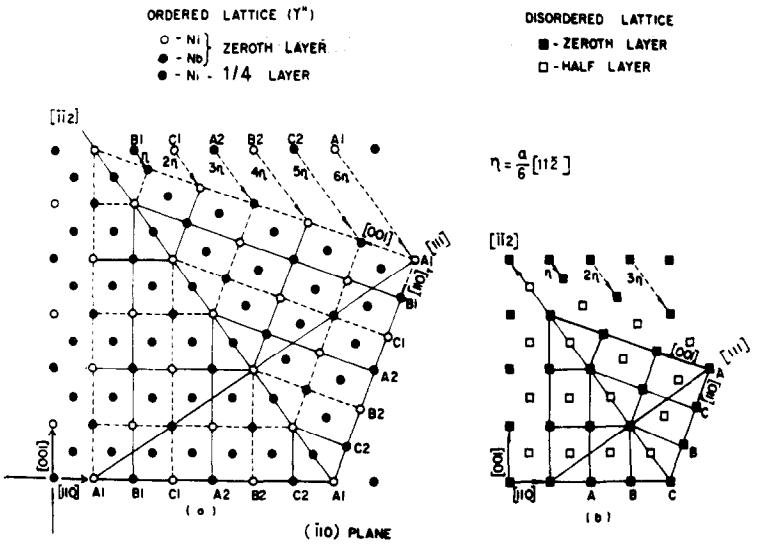

Fig. 18. Schematic illustrations showing $\frac{a}{6}[11\bar{2}]$ shear on every (111) plane in (a) DO_{22} structure and (b) the f.c.c. structure on ($\bar{1}10$) projection. (a) Shows that the new structure produced by such a shear generates a true crystallographic twin, the corresponding superlattice orientations being twin related. (b) Shows twinning produced by the same shear in f.c.c. structure.

As mentioned in Section 2, the DO_{22} structure can be constructed by stacking (111) atomic layers, one above the other, in the six layer sequence $A_1B_1C_1A_2B_2C_2$. Figure 18(a) provides an edge-on view of (111) atomic layers. The open and the closed circles represent M (nickel) and N (niobium) atoms, respectively, on the zeroth layer of the ($\bar{1}10$) plane while crossed circles represent M (nickel) atoms on the one fourth layer. The half layer and the three fourths layers coincide respectively with zeroth and one fourth layers, except for the fact that all atom positions are occupied only by M atoms in these two layers. It can be seen from this construction that the repeat vector along the [111] direction is six times the (111) interplanar spacing. When a $\frac{1}{6}[\bar{1}\bar{1}2]$ displacement is introduced on every plane, a new orientation of the ordered DO_{22} crystal is generated which is twin related to the parent crystal. This is similar to the occurrence of {111} twinning in the A1 structure by the passage of a $\frac{1}{6}\langle\bar{1}\bar{1}2\rangle$ partial dislocation on every {111} layer [Fig. 18(b)]. However, one important point of difference between the geometries of deformation twinning in these two structures must be emphasised. In the case of the A1 structure, shearing along any one of the three equivalent vectors $A\delta$, $B\delta$ and $C\delta$ [Shockley partials lying on the (111) plane] would generate a twin orientation while in the case of the DO_{22} structure, owing to the ordered arrangement of atoms belonging to different species, shearing along only one specific direction in any individual {111} plane would lead to the formation of a twinned crystal. It would be possible for any given precipitate variant to accommodate deformation twins on any one of the four {111} planes since these planes are symmetrically disposed with respect to the tetragonal axis of the precipitate crystal. The corresponding directions of the twinning shear would, however, be different. Table 4 lists the appropriate directions of twin shear for different variants of the precipitates and of twin planes.

Table 4. Twinning shear directions for different variants of precipitates and of twin planes

Precipitate variant c axis parallel to	Twinning shear directions for twin planes (111)	($\bar{1}$11)	(1$\bar{1}$1)	(11$\bar{1}$)
[100]	[2$\bar{1}\bar{1}$]	[211]	[21$\bar{1}$]	[2$\bar{1}$1]
[010]	[$\bar{1}$2$\bar{1}$]	[12$\bar{1}$]	[121]	[$\bar{1}$21]
[001]	[$\bar{1}\bar{1}$2]	[1$\bar{1}$2]	[$\bar{1}$12]	[112]

The observation that precipitates belonging to different variants were twinned predominantly along different {111} planes could be rationalised in terms of the Schmid factor values associated with each of the possible twinning modes for a given tensile stress direction. For precipitates belonging to any particular variant, the twinning mode associated with the most favourable value of the Schmid factor would be preponderantly operative. This mode would correspond to different twin planes in different precipitate variants for any given direction of the tensile stress axis.

It could also be seen from Table 4 that twins on any specific plane of the {111} family can propagate through all the γ'' variants, though the directions of the twinning shear would be different in precipitates belonging to different variants. The orientations of the twinned crystals formed in different variants by such a process would also be different. However, the "average lattice" (disregarding the ordered atomic arrangement in the precipitates) corresponding to these twin crystals would in each instance be identical to that obtained by twinning of the A1 matrix on the same specific {111} plane. This point is illustrated schematically in Fig. 19 by plotting the $\langle 100\rangle_T$ directions of the (111) A1 twin crystal with respect to

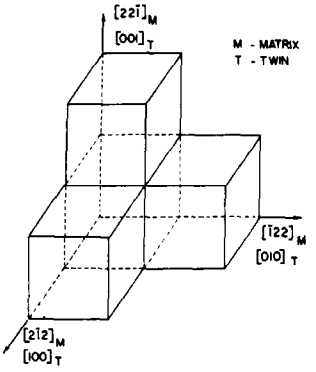

Fig. 19. The relative orientations of the ⟨100⟩ type axes of DO_{22} twin crystals with respect to ⟨221⟩ directions corresponding to the matrix for twinning on a specific (111) plane. The tetragonal axes corresponding to the three variants of twinned crystals are aligned along these three directions. Corresponding tetragonal DO_{22} unit cells are also indicated.

the matrix orientation. The γ'' orientations which are generated by the passage of an (111) deformation twin through γ'' particles belonging to the three variants would then correspond to crystals with their tetragonal axes oriented along the $[100]_T$, $[010]_T$ or $[001]_T$ directions. Such a correspondence between the matrix and the precipitate twins implies that the fundamental reflections associated with all these twin crystals, generated along a given {111} type plane but located within γ'' particles belonging to different variants, would coincide. As a consequence, a dark field image obtained by using a fundamental twin reflection would show all these twin crystals in bright contrast [e.g. Fig. 13(b)].

It is interesting to note that a great majority of deformation twins remained confined within the γ'' particles and did not propagate into the matrix. This observation was suggestive of the fact that the value of the critical resolved shear stress for twinning in the austenite matrix was higher than that in the γ'' precipitates. As pointed out earlier, the SFE of the austenite was larger than that of the γ'' phase and possibly this was the reason why the propagation of deformation twins through the former was relatively difficult. In those instances where a deformation twin did propagate into the matrix and cut across several precipitates along a specific {111} plane, it had to select the appropriate shear directions compatible with the orientations of the precipitate variants in order to conserve the DO_{22} ordering within the twin bands. The mechanism of this process possibly involved a dislocation reaction of the type

$$\delta\mathbf{A} \rightarrow \mathbf{B}\delta + \mathbf{C}\delta$$

where an incoming shear front consisting of a set of $\delta\mathbf{A}$ dislocations on every plane split into sessile $\mathbf{B}\delta$ and glissile $\mathbf{C}\delta$ components at the precipitate–matrix interface. The glissile partials with the appropriate shear vector would glide through a precipitate, leading to twin formation within it. Though the dislocation reaction indicated here is not favourable from dislocation self energy considerations, the energy savings accruing from the preservation of order as the deformation twin propagates may outweigh the energy spent in the creation of a set of sessile partials at the precipitate–matrix interface.

5.4. Effect of γ'' particle size on deformation mode

The present investigation showed that a slip-to-twin transition occurred in the mode of precipitate shearing as the γ'' particle size increased beyond a certain critical value (dimension along the major axis ~ 10 nm). No evidence of dislocation looping around γ'' particles could be obtained though Merrick [17] has mentioned the possibility of the occurrence of looping around fine γ'' precipitates in Inconel 718. The observations made in the work reported here (viz. slip-to-twin transition and non-occurrence of looping) could be rationalised with the aid of Fig. 20 in which the calculated values of the critical shear stress associated with different modes of deformation have been plotted against the γ'' precipitate size.

During the deformation of a two phase aggregate, consisting of a distribution of hard, ordered particles in a softer matrix, two distinct modes of deformation are commonly observed: particle shearing and particle bypassing by the creation of dislocation loops around the particles. The stress required for the former process to occur increases with increasing particle size since the destruction of order over a larger area necessitates the application of a higher stress. The functional relationship between shear stress and particle size for this mode of deformation is given by [11]

$$\Delta\tau = \left[\frac{\Gamma}{2b}\right]\left[\left\{\frac{4\Gamma f R}{\pi T}\left(\frac{\sqrt{6}}{3A}\right)^{1/2}\right\}^{1/2} - \beta f\right] \qquad (2)$$

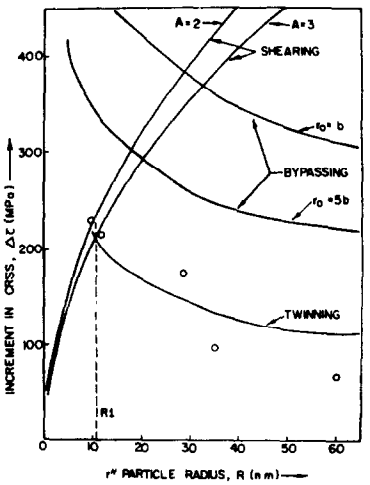

Fig. 20. Calculated values of increment in shear stress, $\Delta\tau$, at 0.2% strain as functions of γ'' particle radius for different deformation mechanisms. Experimentally observed shear stress increments for different particle radii are shown by open circles. R_1 represents the particle radius at which deformation mode of particles changes from shearing to twinning.

where $\Delta\tau$ is the shear stress increment due to particle shearing, Γ is the antiphase boundary (APB) energy of the ordered precipitate phase, b is the Burgers vector of the dislocation which cuts through the precipitates, f is the precipitate volume fraction and T is the dislocation line tension (which is taken to be approximately equal to $\frac{1}{2}\mu b^2$, μ being the shear modulus of the matrix). In the context of γ'' precipitates, the other parameters in equation (2) have the following significance: R is half the average value of the ellipsoidal γ'' particle major axis, A is the aspect ratio given by the ratio of the major and the minor axes and $\beta = 0$ or $\frac{1}{3}$, depending on whether all the precipitates belong to a single variant or whether all the three variants are present in equal numbers. For deformation to occur by the particle shearing mode, matrix dislocations (either **AB** doublets or/and **BC** and **AC** quartets) would be expected to take part in the deformation process. Since dislocation pairs were observed while dislocation quartets were not encountered in the present work, it was assumed that only **AB** dislocation doublets were involved in particle shearing. Shear stress calculations were carried out by using the values $\Gamma = 296\ \mathrm{m\,J\,m^{-2}}$, $\mu = 70\ \mathrm{GPa}$ and $f = 0.1425$, following Oblak *et al.* [11]. Two plots of $\Delta\tau$ vs R were obtained for two values ($A = 2$ and 3) of the aspect ratio (Fig. 20). These values approximately corresponded to experimentally observed values of the largest precipitates deformed by slip and the smallest precipitates deformed by twinning, respectively. The two plots shown in Fig. 20 correspond to $\beta = 0$. It was noted that on putting $\beta = \frac{1}{3}$, the curves were depressed only marginally.

The stress associated with the particle bypassing mechanism decreases with increasing particle size, unlike in the case of the particle shearing mechanism. In precipitation hardening systems, therefore, a point of crossover, in terms of the precipitate size, is generally observed. At precipitate sizes larger than this critical value, the stress requirement for the operation of the bypass mechanism is smaller than that for the shearing process to occur. At smaller particle sizes, however, the situation is reversed. For a constant volume fraction of the γ'' precipitate phase, an increase in the mean precipitate size would be accompanied by a concomitant increase in the mean free spacing between the precipitates and the stress necessary to initiate the bypassing process would decrease according to the relation [36]

$$\Delta\tau = \frac{0.85\,\mu b}{2(1-\nu)^{1/2}} \frac{C}{2R\left[1 - \frac{\pi}{2A}C\right]} \ln\left(\frac{4R}{\pi_0}\right) \quad (3)$$

where $\Delta\tau$ is the shear stress increment associated with precipitate bypassing, ν is the Poisson ratio for the matrix, π_0 is the dislocation core radius and

$$C = \left[(fA)^{1/2} + \left(\frac{2}{\pi} - \frac{\pi}{2A}\right)fA\right]. \quad (4)$$

The other parameters in equation (3) have the same significance as those in equation (2). With continued growth of the ellipsoidal γ'' particles, the aspect ratio would increase continuously. In the present work, the maximum observed value of the mean aspect ratio was about six. In view of this, for calculations on the basis of equation (3), it was assumed that A varied linearly between 2 and 6 with increasing R. The $\Delta\tau$ values associated with Orowan looping were calculated for $\pi_0 = b$ and for $\pi_0 = 5b$. The corresponding plots are shown in Fig. 20.

As described earlier, precipitate shearing through deformation twinning was observed to occur when the precipitate size was not very small. For this mode of particle shearing to start operating, the stress concentration at the precipitate–matrix interface should exceed the stress required to nucleate deformation twins within the γ'' particles. Since the growth of the twin nuclei across the particles would not involve any disruption of order, it would be expected that the growth process would not require a stress higher than the nucleation stress. This implies that once the required threshold stress concentration builds up, the shear would propagate through the precipitate in a catastrophic manner. Such a shear, however, was not manifested as a sudden macroscopic plastic flow and no stress drops were observed in the stress–strain plot. The fact that most of the twins were confined within the numerous fine precipitates distributed uniformly in the matrix appeared to be responsible for rendering the plastic flow, which occurred in bursts in the microscopic scale, homogeneous in both spatial and temporal senses when the scale of observation was macroscopic.

Deformation twinning in the γ'' precipitates in this alloy, which showed a strong tendency for planar slip, was likely to be triggered by the stress concentration developed at the heads of dislocation pile ups in the matrix in the vicinity of γ'' particles. An approximate estimation of the stress required for deformation twin nucleation within a γ'' precipitate could be made by equating the critical stress needed for twin nucleation, τ_T, to the critical stress, τ_c, generated at the head of a dislocation pile-up of length λ which is sufficient to overcome the obstacle against which piling-up occurs. This critical stress can be expressed as [37]

$$\frac{\tau_a}{\mu} = \left(\frac{\tau_c}{\pi\alpha\mu}\right)^{1/2}\left(\frac{\lambda}{b}\right)^{-1/2} \quad (5)$$

where τ_a is the applied shear stress and α is a geometrical factor which assumes a value of 1 for a screw dislocation pile up and of $(1-\nu)$ for an edge dislocation pile up. Expressing λ in terms of R, A and f, and putting $\tau_T = \tau_c$, one could obtain the following relationship (*vide* Appendix)

$$\frac{\tau_a}{\mu} = \left(\frac{15\,b\tau_T}{16\,\pi\mu}\right)^{1/2}\left[\frac{fA}{2R^2}\left(\frac{\pi}{2}\right)^{1/2}\right]^{1/4}. \quad (6)$$

According to this relationship, for constant values of b, μ, τ_T, f and A, τ_a should be inversely proportional to $R^{1/2}$.

As mentioned earlier, the values of the applied shear stress were obtained over a range of γ'' particle sizes (Table 2). The open circles in Fig. 20 correspond to these experimentally obtained points. It could be seen that within the limits of experimental errors, these values were consistent with a $R^{-1/2}$ dependence of τ_a, as predicted by Eq. (5). It has to be mentioned here that a R^{-1} dependence of τ_a could also be fitted reasonably well to the experimental points. Such a dependence would point to the operation of a precipitate bypassing mechanism. However, no TEM evidence for the occurrence of dislocation loops around γ'' particles could be obtained in this work whereas deformation twinning within these particles was very frequently observed. It was felt, therefore, that the $R^{-1/2}$ dependence of τ_a, as suggested by equation (5) was valid here. The flow stress in the deformation twinning regime has been plotted in Fig. 20 on the basis of this analysis. It could be seen from this figure that there existed a precipitate size (e.g. R1) at which the mode of precipitate shear changed from slip to twin. There was a good agreement between the observed and the computed values of this critical size. Below the critical size, the stress required for a pair of **AB** dislocations to cut across a γ'' particle was smaller than that needed to nucleate a deformation twin within it. As the precipitates grew larger, the stress required for particle shearing increased and beyond the critical size, the competitive process of deformation twinning became more favoured. A second important inference that could be drawn from Fig. 20 was that the stress required to bring about deformation twinning in the γ'' particles was lower than that associated with Orowan bypassing for the entire range of precipitate size studied. The largest precipitate size investigated corresponded to the stage where the precipitation of the equilibrium δ phase intervened. Another point that require mention is that a rough estimate of the stress required for twin nucleation (τ_T) could be made from the slope of the τ_a vs $R^{-1/2}$ plot and a value of $\mu/\tau_T \simeq 440$ was obtained, assuming that the shear moduli of the austenite and the γ'' phases were equal. This value compared reasonably well with the experimentally determined values of twin nucleation stress in some binary alloys [38] and pure metals [39] with the A1 structure.

5.5. Work-hardening behaviour

The work-hardening rate in precipitation hardening alloys generally increases abruptly as the precipitate size grows beyond a certain critical value. This effect is attributed to the transition from the precipitate shearing to the precipitate bypassing mechanism regime where deformation results in the accumulation of geometrically necessary dislocations in the vicinity of non-deformable precipitates [40, 41]. In the present case, however, a drop in the work-hardening rate was noticed as the precipitate radius increased beyond a value of about 10 nm. This observation pertaining to the microscopic deformation behaviour of the alloy, strongly suggested that precipitate bypassing mechanisms like Orowan or Hirsch looping did not operate in the present case when the precipitate radius exceeded about 10 nm. The passage of shear through precipitate particles by deformation twinning does not increase the dislocation density of the matrix to any significant extent and consequently this deformation mechanism would not be expected to enhance the work-hardening rate. It is true that deformation twinning of the matrix grains, leading to repeated grain partitioning, is generally responsible for an increase in the work-hardening rate [42]. But in the present case, since deformation twins were mostly confined within precipitate particles, no grain partitioning and the associated increase in work-hardening were encountered. Since the stress required to nucleate deformation twins in precipitate particles is larger than that required for the growth of twins, the nucleation of a bunch of twins would be immediately followed by a "burst" of flow, resulting from the easy propagation of deformation twins across the precipitates. Such microscopic bursts of easy flow did not cause any stress drop in the stress–strain diagram. However, they did manage to bring down the work-hardening rate (work-hardening exponent, $n \approx 0.57$) in this alloy when it contained precipitate particles larger than about 10 nm in radius.

6. CONCLUSIONS

The mechanism of deformation of the nickel base alloy Inconel 718, hardened by γ'' precipitates, has been studied for different sizes of precipitates and the following conclusions have been arrived at:

1. For ellipsoidal γ'' precipitates with mean radius smaller than 10 nm, the deformation through the precipitates occurs by the passage of a group of dislocations which restores order in them.

2. For precipitates with radii larger than 10 nm (up to the largest size investigated, i.e. 60 nm) precipitate shearing occurs by deformation twinning of precipitates.

3. The ordered arrangement (DO_{22} structure) of atoms within the γ'' precipitate crystals is retained within deformation twins which are true crystallographic twins.

4. The change of precipitate shearing mechanism from shearing to that of twinning is accompanied by a drop in the work hardening exponent from ~ 0.8 to ~ 0.5.

5. While the γ' precipitates are often bypassed by the formation of dislocation loops when the particle size exceeds a certain value, similar bypassing mechanism was not observed for the range of γ'' particle sizes studied in this investigation.

6. The flow stress required for deformation twinning of γ'' particles (for the range of particle sizes studied in this investigation) is estimated to be

smaller than that required for the particle bypassing mechanism to operate.

Acknowledgement—The authors are grateful to Dr V. M. Padmanabhan, Dr M. K. Asundi, Mr J. K. Chakrabartty and Mr R. Kishore for many helpful discussions and Dr S. J. Vijayakar for critical reading of the manuscript.

REFERENCES

1. N. S. Stoloff, in *The Superalloys* (edited by C. T. Sims and W. C. Hagel), p. 79. Wiley, New York (1972).
2. L. M. Brown and R. K. Ham, in *Strengthening Methods in Crystals* (edited by A. J. Ardell and R. B. Nicholson), p. 9. Elsevier, Amsterdam (1971).
3. E. Nembach and G. Neitze, *Prog. Mater. Sci.* **29**, 179 (1985).
4. H. Gleiter and E. Hornbogen, *Mater. Sci. Engng* **2**, 285 (1967–68).
5. V. A. Phillips, *Phil. Mag.* **16**, 103 (1967).
6. V. Munjal and A. J. Ardell, *Acta metall.* **23**, 513 (1975).
7. A. J. Ardell, V. Munjal and D. J. Chellman, *Metall. Trans.* **7A**, 1263 (1976).
8. M. C. Chaturvedi, D. J. Lloyd and D. W. Chung, *Metals Sci.* **10**, 373 (1976).
9. W. Huther and B. Reppich, *Z. Metallk.* **69**, 628 (1978).
10. A. J. Ardell, *Metals Sci.* **14**, 221 (1980).
11. J. M. Oblak, D. S. Duvall and D. F. Paulonis, *Metall. Trans.* **5**, 143 (1974).
12. M. C. Chaturvedi and Ya-fang Han, *Metals Sci.* **17**, 145 (1983).
13. D. F. Paulonis, J. M. Oblak and D. S. Duvall, *Trans. Am. Soc. Metals* **62**, 611 (1969).
14. V. Ramaswamy, P. R. Swann and D. R. F. West, *J. less-common. Metals* **27**, 17 (1971).
15. I. Kirman and D. F. Warrington, *Metall. Trans.* **1**, 2667 (1970).
16. D. J. Wilson, *Trans. Am. Soc. Mech. Engrs* **95**, 112 (1973).
17. H. F. Merrick, *Metall. Trans.* **7A**, 505 (1976).
18. D. Fournier and A. Pineau, *Metall. Trans.* **8A**, 1095 (1977).
19. T. H. Sanders, R. E. Frischnuth and G. T. Embley, *Metall. Trans.* **12A**, 1003 (1981).
20. G. Vanderschaeve and B. Escaig, *Physica status solidi* (a) **20**, 309 (1973).
21. G. Vanderschaeve and B. Escaig, *J. Phys. Lett.* **39**, L74 (1978).
22. G. Vanderschaeve and T. Sarrazin, *Physica status solidi* (a) **43**, 459 (1977).
23. A. J. Ardell, *Metall. Trans.* **16A**, 2131 (1985).
24. N. V. Nevitt, in *Electronic Structure and Alloy Chemistry of Transition Elements* (edited by P. A. Beck), p. 169. Interscience, New York (1963).
25. R. E. Smallman, *Modern Physical Metallurgy*, p. 222. Butterworths, London (1970).
26. C. Crussard and B. Jaoul, *Rev. Metals* **57**, 589 (1950).
27. U. F. Kocks, *Metall. Trans.* **1**, 1121 (1970).
28. Ya-fang Han, P. Deb and M. C. Chaturvedi, *Metals Sci.* **16**, 555 (1982).
29. D. W. Pashley and M. J. Stowell, *Phil. Mag.* **8**, 1605 (1963).
30. P. C. J. Gallagher, *Metall. Trans.* **1**, 2429 (1970).
31. P. S. Kotval, *Trans. T.M.S.-A.I.M.E.* **242**, 1651 (1968).
32. B. E. P. Beeston and L. K. France, *J. Inst. Metals* **96**, 105 (1968).
33. L. Delehouzce and A. Deruyttere, *Acta metall.* **15**, 727 (1967).
34. D. R. Muzyka, in *The Superalloys* (edited by C. T. Sims and W. C. Hagel), p. 113. Wiley, New York (1972).
35. P. B. Hirsch and F. J. Humphreys, in *Physics of Strength and Plasticity* (edited by A. S. Argon), p. 189. M.I.T. Press, Cambridge, Mass. (1969).
36. P. M. Kelly, *Scripta metall.* **6**, 647 (1972).
37. J. D. Embury, in *Strengthening Methods in Crystals* (edited by A. Kelly and R. B. Nicholson). Elsevier, Amsterdam (1971).
38. J. A. Venables, in *Deformation Twinning* (edited by R. E. Reed-Hill, J. P. Hirth and H. C. Rogers), p. 77. Gordon & Breach, New York (1964).
39. L. Remy and A. Pineau, *Mater. Sci. Engng* **26**, 123 (1976).
40. D. Raynor and J. M. Silcock, *Metals Sci. J.* **4**, 121 (1970).
41. V. Martens and E. Nembach, *Acta metall.* **23**, 149 (1975).
42. A. M. Garde, E. Angettinger and R. E. Reed-Hill, *Metall. Trans.* **4**, 2461 (1973).
43. J. C. M. Li and Y. J. Chou, *Metall. Trans.* **1**, 1145 (1970).
44. R. T. De Hoff, in *Quantitative Metallography* (edited by R. T. De Hoff and F. N. Rhines), p. 141. McGraw-Hill, New York (1968).
45. P. B. Hirsch and A. Kelly, *Phil. Mag.* **12**, 881 (1965).
46. V. Perovic, G. R. Purdy and L. M. Brown, *Acta metall.* **27**, 1075 (1979).

APPENDIX

The stress experienced by the dislocation at the head of a pile up (equal to the twinning stress) is given by the expression [43]

$$\tau_a = \sqrt{2B\tau_T} \cdot \lambda^{-1/2} \tag{A1}$$

where

$$B = \frac{\mu b}{4\pi} \cdot \frac{(2-\nu)}{(1-\nu)}$$

for a mixed dislocation. All parameters have been defined earlier. Substituting $\nu = \frac{1}{3}$, one obtains

$$B = \frac{5\mu b}{8\pi}. \tag{A2}$$

The value of λ in this case is assumed to be equal to the shortest distance between γ'' precipitates in the slip plane.

Calculation of λ

The number of particles per unit area, N_A, is given by the relation

$$N_A = \frac{f}{(\bar{D}t)} \tag{A3}$$

where $\bar{D}$ is the average diameter of γ'' particles on the slip plane and t is their average thickness. For a thin ellipsoidal precipitate, the area cut by the dislocation will be approximately rectangular. An ellipsoid can be approximated to a disc ($h \ll R$) having the same volume by taking

$$t = \frac{4}{3}h \tag{A4}$$

where h is the semi-minor axis of the precipitate. Dehoff [44] has shown that the expression for the average diameter of a thin ellipsoidal precipitate (which can be approximated to a thin disc) is identical to the expression derived for the average diameter of a sphere measured on an intersecting plane. Hence the expression for the average diameter of a spherical particle [45], namely

$$\bar{D} = \sqrt{\frac{8}{3\pi}} \cdot D \tag{A5}$$

can be used to calculate the average diameter of γ'' particles cut in the slip plane.

Substituting values of $\bar{D}$ and t from equation (A5) and equation (A4) and taking $D = 2R$, the number of particles per unit area can be expressed as

$$N_A = \frac{3f}{16Rh}\sqrt{\frac{3\pi}{2}}. \tag{A6}$$

In this derivation, it is assumed that γ'' particles are distributed in a triangular array in the slip plane. Perovic *et al.*'s [46] study on the stability of arrays of plate shaped precipitates with a tetragonal distortion in a direction normal to their flat faces has confirmed that such an assumption is justified. They have found that the minimum interaction energy corresponds to a situation where the precipitates are naturally perpendicular in the "edge-face" configuration. For such an array, the distribution of precipitates in the slip plane is triangular. The shortest distance, λ, between the precipitates is given by the relation

$$\frac{\sqrt{3}}{2}\lambda^2 N_A = 1. \tag{A7}$$

Substituting for N_A from equation (A6) one arrives at

$$\lambda = \left[\frac{32\,Rh}{9f}\left(\frac{2}{\pi}\right)^{1/2}\right]^{1/2}. \tag{A8}$$

When the expressions for λ and B are substituted in equation (A1), one obtains, on simplification, the expression

$$\frac{\tau_a}{\mu} = \left[\frac{15\,b\tau_T}{16\,\pi\mu}\right]^{1/2}\left[\frac{Af}{2\,R^2}\left(\frac{\pi}{2}\right)^{1/2}\right]^{1/4}. \tag{A9}$$